Int J Adv Manuf Technol (2015) 80:1855–1862
DOI 10.1007/s00170-015-7157-4

ORIGINAL ARTICLE

Research on belt grinding for marine propeller blade based on the second-order osculation

Bo Hou[1] · **Yongqing Wang**[1] · **Fengbiao Wang**[1] · **Zhichao Ji**[1] · **Haibo Liu**[1]

Received: 6 September 2014 / Accepted: 12 April 2015 / Published online: 30 April 2015

Abstract An effective method based on the second-order osculation principle is developed for grinding surface in this paper. On the assumption that the elastic contact wheel of abrasive belt grinder is a rigid body, the calculation of the contact wheel posture, the maximum width of the grinding belt, and grinding path are described in detail. Since the contact wheel touches the workpiece surface in line, the deformation of the contact wheel is uniform under the grinding pressure. Then an offset surface can be obtained by translating the tracing surface of the tool axis, and it can approach the machined surface more closely in the grinding process; thus, the precision and efficiency of the machining can be improved effectively. Finally, some machining examples are carried out on a developed five-axis computer numerical control (CNC) belt grinding machine, and the experimental results verify that the proposed method is practical and efficient.

Keywords Marine propeller blades · Belt grinding · The second-order osculating

Nomenclature

$\dot{R}$	Material removal rate
K	Constant related to belt type, workpiece material, and other factors
V	Grinding speed
T	Grinding time
F	Acting pressure between contact wheel and workpiece
MR(T)	Material removal amount
h_a	Actual grinding depth
h_t	Theoretical grinding depth
Δh	Elastic deformation of contact wheel
δ	Total depth error caused by other factors including belt wear, the rigidity of machine tools and the workpiece, abrasive particles, and so on
ξ_1	A local coordinate system on the blade
O^B	Original point of the Frenet frame ξ_1
e_1^B	Unit binormal vector of the blade surface
e_2^B	Principal unit tangent vector of the blade surface
e_3^B	Unit normal vector of the blade surface
ξ_2	A local coordinate system on the contact wheel
O^W	Original point (the center of the contact wheel)
e_1^W	Unit binormal vector of the local coordinate ξ_2
e_2^W	Tool radial vector pointing to the support axis of the contact wheel
e_3^W	Tool axis vector of the contact wheel
e^P	Projection of e_3^W, belongs to the tangent plane consisted of vector e_2^B and e_3^B
α^B	Included angle between the projection line e^P and the vector e_2^B
β^W	Angle between projection line e^P and tool axis e_3^W
T^E	Intersection point of e_3^B and e_3^W
M	Distance between point O^B and point T^E
N	Distance between point O^W and point T^E
ξ_m	A local coordinate system on at the point O^B
m_1^B, m_2^B	Unit vectors of the surface along the principal directions at point O^B
α	Angle between e_3^W and m_1^B
k_1, k_2	Principal curvatures of the point O^B of the machined surface

✉ Bo Hou
bhou@mail.dlut.edu.cn

[1] Key Laboratory for Precision and Non-traditional Machining Technology of Ministry of Education, Dalian University of Technology, No.2, Linggong Road, Dalian 116024, People's Republic of China

σ_h	Residual error of the second-order osculation method
n_f	Unit vector along direction of machined
n_t	Unit vector along the osculating direction
φ	Angle between t and m_1
c	Machining path $c=c(u(s),v(s))$
c_s	Unit tangent vector of the machining path
Δs	Step length of grinding
Σ_g	Surface of the contact wheel
Σ_S	Machining surface
Σ_t	Tracing surface generated by tool axis moving
Σ_O	Offset surface of the tracing surface Σ_t

1 Introduction

Belt grinding is one of the most effective ways for finishing machining with higher dimensional accuracy and better surface quality [1, 2] and very suitable for producing workpiece surfaces with complex geometrical shapes, such as free-form surface blades [3, 4]. At present, marine propeller blades are grinded by hand due to the complexity of its shapes, which wastes too much time and efforts. To increase production efficiency and improve surface quality, CNC belt grinding machines are recently introduced in the free-form surface grinding process [5, 6]. However, the inhomogeneity of the elastic deformation in the contact wheel will decrease the surface quality of the workpiece in the traditional CNC belt grinding process; thus, how to maintain uniform deformation of the contact wheel is critical for the surface quality and grinding efficiency.

For belt grinding operation, very few published literatures are available; Zhsao and Shi designed a pneumatic flexible polishing force-exerting mechanism and proposed a dual-mode switching composite adaptive control (DSCAC) strategy [7]. Shi and Zhang proposed the control method of the sixth axis by the principles of interference-free, effective space, and maximum cutting strip [8]. Zhang et al. presented a new model based on a neural network technique to calculate the force distribution in the contact area between the workpiece and elastic grinding wheel. The new model was executed much faster than finite element model (FEM) and real-time simulation, and online robot control of grinding processes can be further conducted [9, 10]. Ren and Kuhlenkötter proposed a new free-form surface representation based on discrete element method that is developed to facilitate the system implementation. A local process model was integrated to calculate the material removal rate by considering the local geometry information and non-uniform force distribution [11]. Wu et al. presented a platform for comprehensive modeling and simulation of the robotic belt grinding system. The system simulation showed that optimal selection of key control parameters of the grinder and proper selection of robot control strategies can efficiently suppress chatter in the grinding process. A material removal model of the grinding process, which can adapt to workpieces with complicated shapes, was also developed and presented [12]. To develop a high-quality robot grinding system, Song et al. proposed an off-line planning method for the control parameters of the grinding robot based on an adaptive modeling method [13]. Sun et al. describes a novel methodology for robotic belt grinding, which primarily focuses on system calibration and force control to improve grinding performance [14].

Belt grinding has been investigated for decades. However, very few research of belt grinding for complex surfaces have been done, especially contact wheel posture adjusting and grinding path planning which are key factors to improve the surface quality and the grinding efficiency. Due to the similarity between belt grinding and flank milling, path planning method can refer to the way of flank milling. Many methods have been developed to flank milling during the last decades. Wu et al. presented the tool path planning which is transformed into a matching problem between two point sets in 3D space, sampled from the boundary curves of the machined surface [15]. Gong and Wang proposed a global optimization method to generate a tool path for flank milling free-form surfaces with a generic cutter based on approximation using the tool envelope surface [16, 17]. Sprott and Ravani developed a method to generate the tool path with a cylindrical cutter which is based on differential geometry of ruled surfaces in terms of line geometry [18]. Stephen and Radzevich sorted out an integral form of solution to generate optimal tool path [19]. Chiou and Lee carried out a machining potential field (MPF) method to generate tool paths for multi-axis sculptured surface machining [20]. Cao and Liu utilized the second-order osculating machining method to keep cylindrical cutter and the machined surface in line contact [21].

Considering the complexity of the belt grinding and the processing similarity with flank milling, an effective method based on the second-order osculation principle is developed for grinding free-form surface in this paper, especially for finishing large marine propeller. To reduce the errors caused by the non-uniform deformation of the elastic contact wheel, the second-order osculating method is applied to calculate the contact wheel posture and the maximum width of the grinding belt, which makes the contact wheel keep line contact with complex surface. In this situation, the grinding pressure is imposed, and the deformation of the contact wheel is uniform; thus, the errors by deformation can be effectively decreased. In addition, the grinding paths can be worked out for the grinding program with improved machining precision and higher efficiency.

The structure of this paper is as follows: Section 2 presents the belt grinding principle. The second-order osculating machining method of the marine propeller blade is presented in section 3, followed by an

illustrated example in section 4, and the last section is the conclusion.

2 Modeling belt grinding

As shown in Fig. 1, the geometric model of belt grinding is illustrated. The material removal of belt grinding is a complex and statistical process, since a number of abrasive particles with random distribution are generally involved in grinding at the same time.

On the basis of the classical Preston's fundamental polishing equation, the material removal rate $\partial R/\partial t$ of belt grinding can be formulated as,

$$\dot{R} = \partial R/\partial t = KV(t)F(t) \quad (1)$$

where K is constant related to belt type, workpiece material, and other factors. V is grinding speed. F is acting pressure between contact wheel and workpiece [22].

The grinding speed could be configurable, but the acting pressure is not easy to measure and control. For qualitative study of the grinding process, the acting pressure can be obtained by two ways regardless of the local statuses. One method to obtain the acting pressure is through direct measurement under different grinding depth and pressure. As shown in Fig. 2. The acting pressure has been measured by a three-component dynamometer (KISTLER-9257B). The acting pressure in the contact area can also be computed by the finite element method (FEM). Because the contact status can be regarded as a wholly elastic deformation and the classic theoretical model of strain-stress can be applied, it is easy to calculate the deformation information of the elastic contact wheel and indirectly obtained the acting pressure. In short, the acting pressure can be controlled indirectly by regulating the depth of grinding in these two methods. But for accurate partial analysis of the grinding status, the rough linear global relation is no longer adequate. Because the local status of the contact wheel and workpiece involves more process variables such as the local non-uniform pressure distribution, to get information in detail, the FEM model has been established to calculate the grinding pressure distribution. The grinding contact area is divided into a mesh then the local situations on each mesh point are defined. The local pressure under different grinding depth is represented by a matrix on all mesh points.

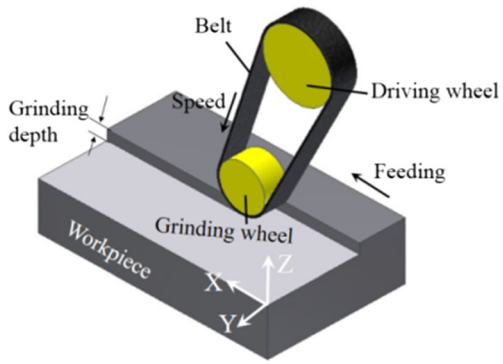

Fig. 1 Geomeric model of belt grinding

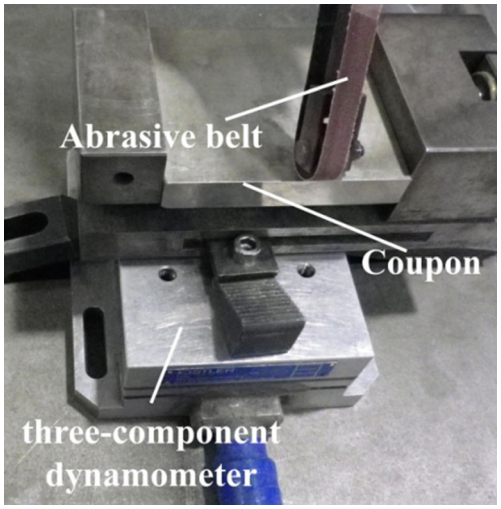

Fig. 2 Measuring the acting pressure of belt grinding

The material removal amount of every point could be accurately calculated by accurate partial analysis of the grinding status. However, it will cause tremendous computational burden and complicate the control system. The global grinding model has been studied to simplify the calculation process. Some assumptions firstly should be given in advance, and it is appropriated as it brings little error:

1. It is only related to the grinding movement of abrasive particles, regardless of the belt motion on the workpiece surface.
2. The grinding wheel remains elastic contact with workpiece during belt grinding, and the wheel deformation is uniform in axial direction. The contact pressure in feed direction is non-uniform distribution.
3. More material would be removed within longer grinding time.

The material removal rate distribution could be calculated according to the formula (1). Figure 3 has shown the material removal rate distribution of belt grinding. The $\partial R/\partial t$ of each point decreases gradually with grinding wheel elastic resilience. The material removal rate distribution is not symmetric, and the maximum value of material removal rate is slightly off-center. This is because the pressure of this point reached the maximum during the grinding machining.

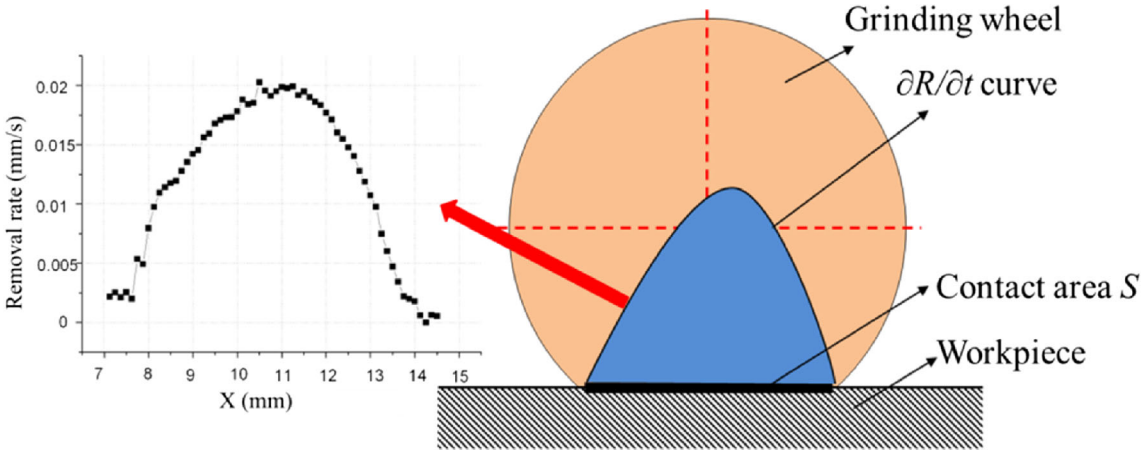

Fig. 3 Removal rate of belt grinding

Thus, the material removal is a dynamic process. The material removal amount MR(T) of each grinding point in contact area is an integration in grinding time T,

$$\mathrm{MR}(T) = \int \dot{R}\mathrm{d}t = K\int_0^{\mathrm{T}} V(t)F(t)\mathrm{d}t \tag{2}$$

where T can be called grinding dwell time, dt is the time integration increment.

According to the material removal rate distribution and assumptions, a two-dimensional (2D) belt global grinding model can be established with material removal rate and grinding dwell time. The global grinding model, which is not only applied to manufacturing of simple-shaped workpiece surfaces and also can be applied to qualitative study of the grinding process, considers the workpiece as a whole, regardless of the local statuses.

Indeed, the actual grinding depth h_a at each point is a direct factor to control target surface. However, it is unavoidable that h_a is smaller than the theoretical grinding depth h_t due to the elastic contact, formulated as:

$$h_a = h_t - (\Delta h + \delta) \tag{3}$$

where Δh is the elastic deformation of contact wheel, δ is total depth error caused by other factors including belt wear, the rigidity of machine tools and the workpiece, abrasive particles, and so on.

The material removal $\dot{R}$ is proportional to elastic deformation Δh. Thus, non-uniform deformation of the contact wheel leads to non-uniform material removal, causing machining errors.

In conclusion, the belt grinding processing method is supposed to be the same with side milling in the condition of non-contact stress. The pose of the contact wheel was adjusted to ensure the contact wheel and workpiece with line-contact. And then, the contact pressure was exerted to make the contact wheel deformation uniform. The second-order osculating method applied in side milling processing shared similarities with belt grinding. Based on this method, the pose of contact wheel and feed direction were calculated.

3 The second-order osculating grinding method of the marine propeller blade

The idea of the second-order osculating method is that the normal plane which goes through a point on the machined surface along the direction of the osculating plane has section curves with workpiece and tool surface separately; these two lines have the same cross-sectional curvature at this point. Calculation about the position of the tool at some point is looking for the direction of osculating and the corresponding tool axis direction [20].

An arbitrary point O^B on the blade is taken as its machining start point. As shown in Fig. 4, at point O^B, a local coordinate system $\xi_1=\{O^B;e_1^B,e_2^B,e_3^B\}$ is established. O^B is the original

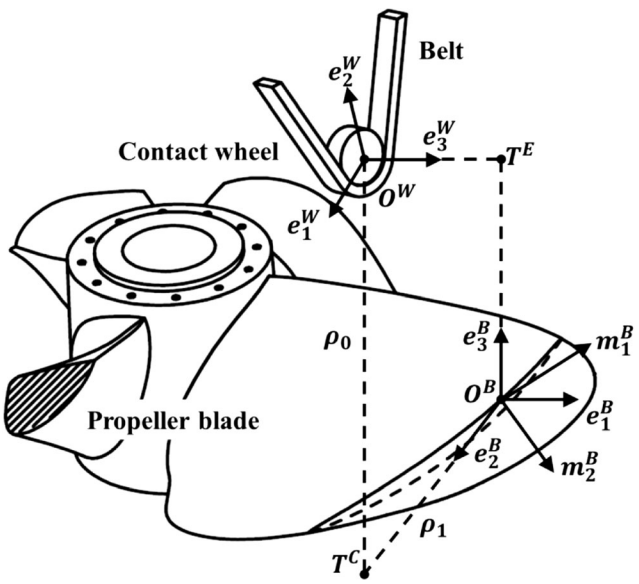

Fig. 4 Tool pose

point of the Frenet frame ξ_1. e_2^{B} is the unit tangent vector and e_3^{B} is the unit normal vector of the curved surface. On the contact wheel, $\xi_2=\{O^{\mathrm{W}};e_1^{\mathrm{W}},e_2^{\mathrm{W}},e_3^{\mathrm{W}}\}$ is defined to be the Frenet frame, O^{W} is the original point (the center of the contact wheel), and e_3^{W} is the tool axis vector of the contact wheel, and e_2^{W} is the tool radial vector pointing to the support axis of the contact wheel. The relations of ξ_1 and ξ_2 can be expressed as:

$$\begin{cases} e_1^{\mathrm{W}} = \sin\beta^{\mathrm{W}}\left(e_1^{\mathrm{B}}\cos\alpha^{\mathrm{B}} + e_2^{\mathrm{B}}\sin\alpha^{\mathrm{B}}\right) - e_3^{\mathrm{B}}\cos\beta^{\mathrm{W}} \\ e_2^{\mathrm{W}} = -e_1^{\mathrm{B}}\sin\alpha^{\mathrm{B}} + e_2^{\mathrm{B}}\cos\alpha^{\mathrm{B}} \\ e_3^{\mathrm{W}} = \cos\beta^{\mathrm{W}}\left(e_1^{\mathrm{B}}\cos\alpha^{\mathrm{B}} + e_2^{\mathrm{B}}\sin\alpha^{\mathrm{B}}\right) + e_3^{\mathrm{B}}\cos\beta^{\mathrm{W}} \end{cases} \tag{4}$$

where α^{B} is the included angle between the projection line e^{P} and the vector e_2^{B}. The projection line e^{P} which is the projection of e_3^{W}, belongs to the tangent plane consisted of vector e_2^{B} and e_3^{B}, β^{W} is the angle between projection line e^{P} and tool axis e_3^{W}. These two parameters α^{B} and β^{W} describe the pose of the contact wheel under Frenet frame ξ_1.

The equation of the contact wheel in the absolute coordinate can be written as:

$$\rho_0 = \rho_1 + Me_3^{\mathrm{B}} + Ne_3^{\mathrm{W}} \tag{5}$$

where M is the distance between point O^{B} and point T^{E}, T^{E} is the intersection point of e_3^{B} and e_3^{W}, and N is the distance between point O^{W} and point T^{E}.

The adjustment of parameter ρ_0, α^{B} and β^{W} are needed to make the contact wheel tangent with the propeller blade on point O^{B}.

Frenet frame $\xi_m=\{O^{\mathrm{B}};m_1^{\mathrm{B}},m_2^{\mathrm{B}},m_3^{\mathrm{B}}\}$ is established at point O^{B}, as shown in Fig. 5. Where m_1^{B} and m_2^{B} are the unit vectors of the surface along the principal directions at point O^{B}, and e_3^{B} is the common normal vector.

The posture of the contact wheel is determined by the angle α between e_3^{W} and m_1^{B}, the angle α can be written as:

$$\cos^2\alpha = \frac{k_1k_2 - k_2k_t}{k_1k_t - k_2k_t} \tag{6}$$

where k_1 and k_2 denote the principal curvatures of the point O^B of the machined surface, and $k_t=1/r$.

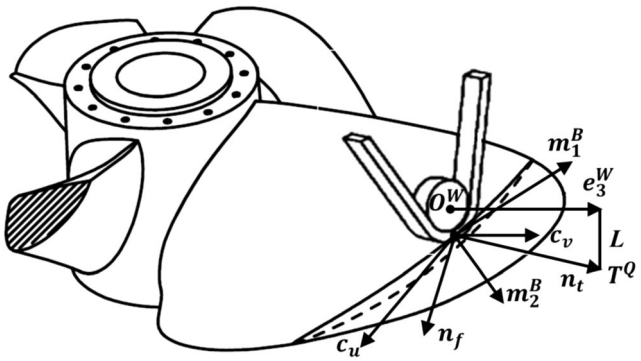

Fig. 5 Principle of the second-order osculating method

According to the second-order osculation principle, it is known that when the direction of feed orthogonal intersects with the osculating direction, the residual error σ_h reaches its minimum value, while the strip width reaches its maximum value [21]. n_f is the unit vector along the direction of machined; n_t is the unit vector along the osculating direction,

$$n_f = n_t \times e_3^{\mathrm{B}} \tag{7}$$

φ is the angle between n_t and m_1^{B}, which determined the grinding direction. The equation can be written as:

$$\tan^2\varphi = \frac{k_t\sin\alpha\cos\alpha}{k_t\cos^2\alpha - k_2} \tag{8}$$

The machining path c can be expressed as $c=c(u(s),v(s))$, and c_s is the unit tangent vector of the machining path,

$$c_s = \dot{c} = c_u\frac{du}{ds} + c_v\frac{dv}{ds} = c_u\frac{\Delta u}{\Delta s} + c_v\frac{\Delta v}{\Delta s} \tag{9}$$

$$\begin{cases} c_s \cdot n_t = 0 \\ c_s \cdot n_f = 1 \end{cases} \tag{10}$$

Since the step length of grinding Δs is given, the increments Δu and Δv of the parameters u and v can be calculated. Substituting Eqs.7, 8, and 9 into Eq. 10, Δu and Δv can be written as:

$$\begin{cases} \Delta u = \dfrac{c_v \cdot n_{\mathrm{t}}}{(c_u \times c_v)\cdot e_3}\Delta s \\ \Delta v = \dfrac{c_u \cdot n_t}{(c_u \times c_v)\cdot e_3}\Delta s \end{cases} \tag{11}$$

Therefore, we obtain the next grinding point location. And then, the position of contact wheel and optimal direction of feed on the new grinding point are calculated. The next grinding point is found in order to form the grinding boot path.

In the process of machining, according to Eqs. 5 and 6, the position of contact wheel is calculated on each grinding point. The surface of the contact wheel Σ_{g} always keeps tangent contact with the machining surface Σ_S during the contact wheel moving according to the machining path c. As shown in Fig. 6, the tool axis will generate a tracing surface Σ_{t}. When the contact pressure F is applied, the position of the center of the contact wheel is

$$\rho_c = \rho_1 + Re_3^{\mathrm{B}} - \Delta h' \tag{12}$$

where R denotes the radius of the contact wheel. $\Delta h'$ is the elastic deformation of the contact wheel.

Then,

$$\Delta h' = \Delta h - \sigma_h \tag{13}$$

Σ_{O} is the offset surface of the tracing surface Σ_{t}. During the grinding process, the offset surface Σ_{O} approaches the

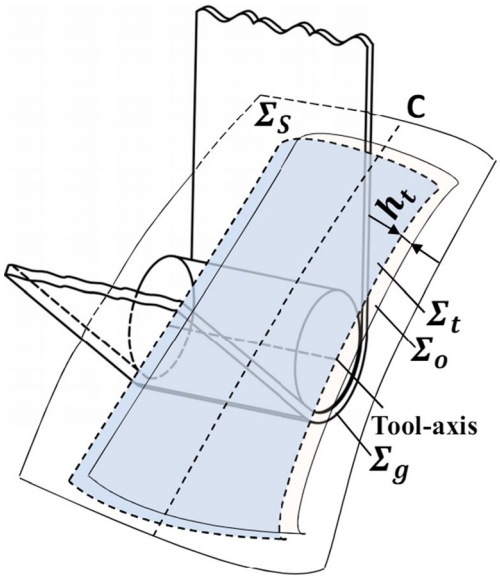

Fig. 6 The model of machining complex surface by using abrasive belt

machined surface Σ_S as close as possible, and the deform uniformity of the contact wheel is obtained.

Generally, by using this method, the contact wheel touches the workpiece surface in line. After the grinding path is calculated, the tool axis will generate a tracing surface Σ_t which approaches the machined surface Σ_S more closely. Then the acting pressure is applied, the deformation of the contact wheel is uniform, and the tool axis will generate a new offset surface Σ_t. In the grinding process, the offset surface Σ_t can approach the machined surface as close as possible.

4 Illustrated examples

The marine propeller is a large complex surface. However, the high-dimensional accuracy and surface quality are very difficult to obtain in the finishing stage due to non-uniform machining allowance and high-toughness material. Further, a five-axis CNC belt grinding machine that integrated measuring and machining has been developed, shown in Figs. 7 and 8. The machine is mainly composed of gantry structure, belt grinding equipment, measuring devices, rotary table, and fixtures. The axes are defined as two linear axes including X-axis and Z-axis and three rotary axes including A-axis, C1-axis, and C2-axis.

The belt grinding equipment has a driving wheel, a contact wheel, and a tension accessory. As shown in Fig. 6, the abrasive belt covers the contact wheel and is driven by the driving wheel with some pre-load generated by the tension accessory. During the machining, the workpiece is pushed against the contact wheel. The distributed abrasive grains, which are bounded by special mediums on a bedding layer of the belt, act as the cutting edges to remove materials.

In this paper, a right-handed propeller in diameter 2400 mm is taken for an example to illustrate the tool path planning method. The marine propeller is shown in Fig. 9. The marine propeller material is cast aluminum bronze material (ZCuAl9Fe4Ni4Mn2). Tensile strength is 630 MPa, yield strength is 250 MPa, and hardness is 1570 HB. The wheel material is rubber with Poisson's ratio 0.47, elastic modulus 7.8 GPa, and yield strength 9.24 MPa. The abrasive belt size is 533 mm×9 mm. The abrasive belt is 150#. The grinding depth is 0.5 mm, the feed rate is 140 mm/min, and the grinding speed is 1420 m/min. The ratio of propeller pitch to the diameter is 0.652. The rake is 10°. The boss ratio is 0.176. Firstly, the actual propeller shape is measured on-machine using a laser sensor. Further, by the second-order osculating method, the posture of contact wheel and the belt grinding path are calculated. The grinding parameters (such as speed, feed, etc.) are programmed on the basis of the proposed control strategy. Finally, the belt grinding is implemented.

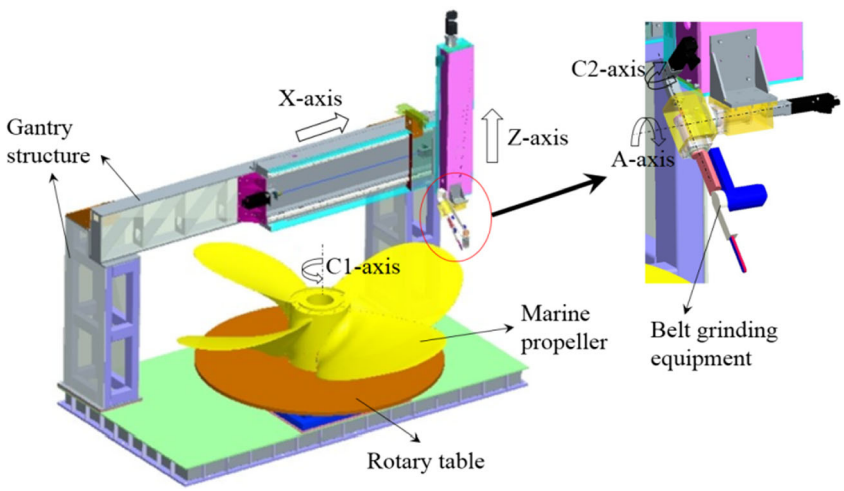

Fig. 7 Five-axis CNC belt grinding machine schematic

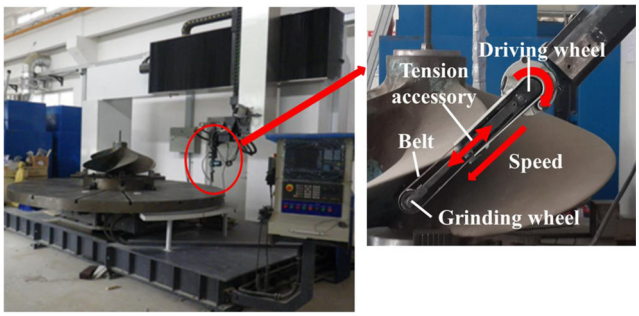

Fig. 8 CNC belt grinding machine and belt grinding equipment

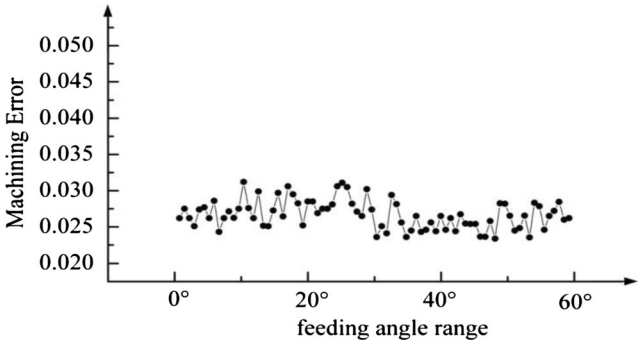

Fig. 10 Machining error (R=1050 mm)

The propeller blade tip zone π (R=1000–1100 mm) had been used for experimental validation, as shown in Fig. 9. The thickness of machined material was estimated by comparing the measured blade profile and the designed blade profile. As an example, the machining error along the grinding path L is shown in Fig. 10, radius was 1050 mm, and the feeding angle range was from 0° to 59.2°.

For a given tolerance ($-0.3\text{mm}<\Delta Z<+0.3\text{mm}$), the machining error is less than 0.035 mm which is fairly small. There are many factors causing errors of blades during belt grinding machining. One reason is belt wear, which lead to the decrease of the material removal capability. The hardness of the rubber contact wheel and the stiffness of the arm of the belt grinder also affect machining accuracy. The hard contact wheel and low stiffness of the arm will lead to mechanical vibrations which cause the machining error.

During the grinding process, every parameter to be studied during the grinding process is quantified by only one value, such as grinding speed, grinding depth, dwell time, etc. But the machining allowance of each point is different. This is because the blade surface has been milled as a rough machining. Inevitably, there are uneven distributions of machining allowance. Belt grinding is characterized by elastic contact grinding. It is difficult to meet the grinding requirements under same grinding parameters. This is the key reason of the machining error. Future study should force on an effective method that can control the material removed process of belt grinding for complex surfaces based on effective simulation of grinding status and reasonable dwell time. Based on the second-order osculating method, the contact wheel posture is adjusted to the blades surface feature accordingly, and the grinding parameters are also adjusted in real time to control the material remove rate.

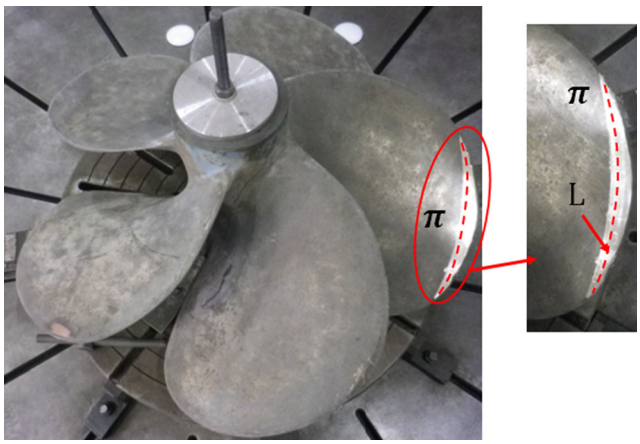

Fig. 9 The grinded propeller blade tip zone π

5 Conclusions

In five-axis CNC abrasive belt grinding machines, non-uniform deformation of the contact wheel leads to non-uniform material removal and thus brings to the machining errors. To overcome this issue, an effective method based on the second-order osculation principle was proposed for grinding free from surface. In this method, considering the characteristics of belt grinding, the contact wheel posture is adjusted at grinding point to uniform deformation and reduce the grinding errors, based on which the optimal feed direction is obtained, and the maximum width of the grinding belt is worked out to improve efficiency. This method was verified on a five-axis CNC belt grinding machine, and the results showed that the machining error is smaller than the given tolerance, and the machining precision and efficiency could be improved in the machining of propeller with larger area ratio.

For grinding error, there are many factors causing it, such as belt wear, the stiffness of the arm of the belt grinder, grinding parameters, and dwell time. In a future study, we will consider surface geometry, grinding force and system stiffness in surface belt grinding, and optimize the grinding parameters (such as speed, feed, etc.) to enhance the overall accuracy thoroughly.

Acknowledgments The authors would like to gratefully acknowledge the financial support from the National Basic Research Program of China (No.2014CB046604), the National Nature Science Foundation of China (No.51305062),

References

1. Axinte DA, Kritmanorot M, Axinte M, Gindy NNZ (2005) Investigations on belt polishing of heat-resistant titanium alloys. J Mater Process Technol 166(3):398–404
2. Axinte DA, Kwong J, Kong MC (2009) Workpiece surface integrity of Ti-6-4 heat-resistant alloy when employing different polishing methods. J Mater Process Technol 209(4):1843–1852
3. Xiao G, Huang Y (2015) Constant-load adaptive belt polishing of the weak-rigidity blisk blade. Int J Adv Manuf Technol 2015:1–12
4. Zhihui GAO, Xiaodong LAN, Yushu B (2011) Structural dimension optimization of robotic belt grinding system for grinding workpieces with complex shaped surfaces based on dexterity grinding space. Chin J Aeronaut 24(3):346–354
5. Wang J, Zhang D, Wu B, Luo M, Zhang Y (2015) Kinematic analysis and feedrate optimization in six-axis NC abrasive belt grinding of blades. Int J Adv Manuf Technol 2015:1–10
6. Liu ZY, Huang Y, Wei HP, Chao S (2013) Research on the technology of NC abrasive belt grinding for the leading and trailing edges of aero-engine blades. Adv Mater Res 797:67–72
7. Zhsao P, Shi Y (2013) Composite adaptive control of belt polishing force for aero-engine blade. Chin J Mech Eng 26(5):988–996
8. Shi J, Zhang Q (2010) Determination of contact wheel position and orientation for six-axis blade CNC abrasive belt grinding system. Mech Sci Technol Aerosp Eng 29(2):196–200
9. Zhang X, Kneupner K, Kuhlenkötter B (2006) A new force distribution calculation model for high-quality production processes. Int J Adv Manuf Technol 27(7-8):726–732
10. Zhang X, Kuhlenkötter B, Kneupner K (2005) An efficient method for solving the Signorini problem in the simulation of free-form surfaces produced by belt grinding. Int J Mach Tool Manuf 45(6): 641–648
11. Ren X, Kuhlenkötter B (2008) Real-time simulation and visualization of robotic belt grinding processes. Int J Adv Manuf Technol 35(11-12):1090–1099
12. Wu S, Kazerounian K, Gan Z, Sun Y (2013) A simulation platform for optimal selection of robotic belt grinding system parameters. Int J Adv Manuf Technol 64(1-4):447–458
13. Song Y, Liang W, Yang Y (2012) A method for grinding removal control of a robot belt grinding system. J Intell Manuf 23(5):1903–1913
14. Sun Y, Giblin DJ, Kazerounian K (2009) Accurate robotic belt grinding of workpieces with complex geometries using relative calibration techniques. Robot Comput Integr Manuf 25(1):204–210
15. Wu PH, Li YW, Chu CH (2008) Optimized tool path generation based on dynamic programming for five-axis flank milling of rule surface. Int J Mach Tool Manuf 48(11):1224–1233
16. Gong H, Wang N (2010) Optimize tool paths of flank milling with generic cutters based on approximation using the tool envelope surface. Comput Aided Des 41(12):981–989
17. Gong H, Wang N (2011) 5-Axis flank milling free-form surfaces considering constraints. Comput Aided Des 43(6):563–572
18. Sprott K, Ravani B (2008) Cylindrical milling of ruled surfaces. Int J Adv Manuf Technol 38:649–656
19. Radzevich SP (2006) A closed-form solution to the problem of optimal tool-path generation for sculptured surface machining on multi-axis NC machine. Math Comput Model 43(3-4):222–243
20. Chuang-Jang C, Yuan-Shin L (2002) A machining potential field approach to tool path generation for multi-axis sculptured surface machining. Comput Aided Des 34:357–371
21. Lixin C, Jian L (2008) An integrated surface modeling and machining approach for a marine propeller. Int J Adv Manuf Technol 35: 1053–1064
22. Preston FW (1927) Glass technology. J Soc Glas Technol 11:277–281